Biaxial disclinated states in nematic elastomers

Eliot Fried
Department of Mechanical Engineering, Washington University in St. Louis, St. Louis, Missouri 63130-4899 and Department of Theoretical and Applied Mechanics, University of Illinois at Urbana-Champaign, Urbana, Illinois 61801-2935

Vladimir Korchagin and Russell E. Todres
Department of Theoretical and Applied Mechanics, University of Illinois at Urbana-Champaign, Urbana, Illinois 61801-2935

(Received 24 July 2003; accepted 4 September 2003)

We use a continuum model to investigate the isochoric axial contraction and expansion of a right circular cylindrical specimen composed of a nematic elastomer that is cross-linked in a uniaxial state and then annealed. We build on previous work by relaxing the constraint that the molecular conformation be spherical or uniaxial, allowing instead for biaxiality. The material exhibits an energetic preference for states involving a disclination of strength $+1$ along the cylinder axis surrounded by a region in which the conformation of the polymer chains is indeed biaxial. We show that such states represent minimizers of the total free-energy. Also, the reactive pressure necessary to enforce the constraint of material incompressibility within the disclination core is found to be reduced by an order of magnitude when the conformation is biaxial rather than uniaxial. A bifurcation analysis is used to analytically determine the thresholds of axial expansion and contraction at which the material prefers a disclinated state. These thresholds are found to be consistent with numerical predictions. Finally, the stability of the solutions for the studied parameters is also investigated. © *2003 American Institute of Physics.* [DOI: 10.1063/1.1622374]

I. INTRODUCTION

Disclinations and defects play an important role in traditional nematic liquid crystals and are expected to be equally influential in nematic elastomers. Previously,[1–3] we used a continuum model to investigate both the existence and detection of disclinations of strength $+1$ induced by the isochoric distortion of a right circular cylindrical specimen composed of a nematic elastomer that is cross linked in a uniaxial state and then annealed. Under deformation, rather than remaining in its annealed, isotropic, reference state, we found that there is an energetic preference for the material to achieve a disclinated state consisting of an isotropic core surrounded by an anisotropic region in which the conformation of polymer chains was uniaxial. Furthermore, by investigating the first normal-stress difference, we proposed a practical method for detecting the onset of a disclinated state.

Our previous work only allowed for a uniaxial molecular conformation. Here, although prepared with a uniaxial conformation as before, the polymer chains are permitted to take on biaxial conformations. From our earlier investigations, we know that, when sufficiently deformed, a nematic-elastomeric cylinder will exhibit a disclination. This work is motivated by the question as to whether the conformation of polymer chains in the region surrounding the core of such a disclination is uniaxial or become biaxial. If this extra-core region is uniaxial, there is then no need to allow for biaxiality. However, if this extra-core region is biaxial, we can conclude that a model in which the conformation is constrained to be either sperhical or uniaxial overly restrictive and that allowing for biaxiality is a necessary refinement.

To describe biaxiality, we introduce scalar asphericities $q_1 > -1$ and $q_2 > -1$ and associated unit orientations $\mathbf{n}_1$ and $\mathbf{n}_2$. The chains are oblate about $\mathbf{n}_1$ for $-1 < q_1 < 0$; spherical for $q_1 = 0$; and prolate about $\mathbf{n}_1$ for $q > 0$. Analogous interpretations hold for q_2 and $\mathbf{n}_2$. In our theory, the asphericities and orientations have the status of additional kinematical degrees of freedom. These lead to balances for aspherical and orientational forces that are enforced in addition to the standard balance associated with the deformational balance. The first asphericity q_1 and orientation $\mathbf{n}_1$ correspond to q and $\mathbf{n}$ in our previous work.[1–3] Thus, if in deforming a nematic-elastomeric cylinder, we find that $q_1 \neq 0$ and $q_2 = 0$ in the extra-core region, we can infer that the disclination is uniaxial. However, if both $q_1 \neq 0$ and $q_2 \neq 0$ in the extra-core region, the disclination is biaxial.

In fact, for both radial expansion and contraction of such a cylinder, we do indeed discover disclinated states in which the conformation of the region surrounding the core is biaxial. Such states possess lower total free energy than those in which the conformation is uniaxial or isotropic. Thus, we find that there is an energetic incentive for disclinated states involving an extra-core region that is biaxially rather than uniaxially anisotropic. Furthermore, we find that in a biaxially disclinated state the pressure necessary to maintain the constraint of material incompressibility within the disclination core is generally an order of magnitude less than that necessary in a uniaxially disclinated state.

These results are obtained via numerical studies of the governing boundary-value problem. To explore their basis, we perform bifurcation and stability analyses of the underlying differential equations. These analyses yield expressions

for the threshold values of axial contraction and expansion for which biaxial states are preferred and these expressions confirm our numerical results.

II. THEORY

The kinematical description of a nematic elastomer involves two fields: the vector-valued deformation $\mathbf{y}$ and the positive-definite and symmetric molecular conformation $\mathbf{A}$, a macroscopic measure of the nematically induced distortion of the polymer chains comprising the network. Associated with $\mathbf{y}$ is the deformation-gradient $\mathbf{F}=\mathrm{Grad}\,\mathbf{y}$, which serves as a macroscopic measure of the distortion of the network. Assuming that the medium is incompressible, we must have $\det\mathbf{F}=1$. Being positive-definite and symmetric, $\mathbf{A}$ in general possesses three distinct eigenvalues and eigenvectors and, thus, may be spherical, uniaxial, or biaxial. When $\mathbf{A}$ is spherical, the medium behaves as conventional isotropic rubber. Otherwise, the optical–mechanical response of the material is anisotropic. In general, we may represent $\mathbf{A}$ in the form

$$\mathbf{A}=a(1+q_1)^{-1/3}(1+q_2)^{-1/3}(\mathbf{1}+q_1\mathbf{n}_1\otimes\mathbf{n}_1+q_2\mathbf{n}_2\otimes\mathbf{n}_2), \tag{1}$$

with $\det\mathbf{A}=a>0$, scalar asphericities $q_\beta>-1$, $\beta=1,2$, and orientations $\mathbf{n}_\beta$ which are orthogonal ($\mathbf{n}_1\cdot\mathbf{n}_2=0$) and of unit length ($|\mathbf{n}_\beta|=1$). The polymer chains are oblate, spherical, or prolate about $\mathbf{n}_\beta$ as $-1<q_\beta<0$, $q_\beta=0$, or $q_\beta>0$, respectively.

Within the molecular-statistical framework of Warner *et al.*,[4] the coupling between the kinematical degrees of freedom is embodied by a free-energy density of the form

$$\tfrac{1}{2}\mu(|\mathbf{A}^{-1/2}\mathbf{F}\boldsymbol{\Lambda}^{1/2}|^2-\ln\det(\mathbf{A}^{-1}\boldsymbol{\Lambda})-3). \tag{2}$$

Here, $\mu>0$ is the shear modulus and $\boldsymbol{\Lambda}$ is the positive-definite and symmetric molecular conformation at the time of crosslinking. While μ would be determined by conventional mechanical tests, $\boldsymbol{\Lambda}$ would be determined using scattering methods. When $\mathbf{A}=\boldsymbol{\Lambda}=a\mathbf{1}$, (2) reduces to the classical expression $\frac{1}{2}\mu(|\mathbf{F}|^2-3)$ of neo-Hookean rubber elasticity.

We consider a nematic elastomer formed by a two-step process as follows: First, the melt is crosslinked in a uniaxial state with asphericity $q_*\neq0$ and unit orientation $\mathbf{n}_*$; next, the resulting network is annealed, giving rise to an isotropic reference state in which the conformation at each material point is of the spherical form $\boldsymbol{\Lambda}=\alpha\mathbf{1}$. In addition to possessing an energetic preference for the isotropic reference state, we assume that the material possesses an energetic preference for states in which either or both of the asphericities adopt the value q_* present at the time of crosslinking. However, we assume that the annealing process renders negligible any energetic preference for the orientation axis $\mathbf{n}_*$ of the molecular conformation at the time of crosslinking. To describe such a material, we incorporate (2) and consider a free-energy density of the form

$$\begin{aligned}\psi=\frac{\mu}{2}\Bigg(&(1+q_1)^{1/3}(1+q_2)^{1/3}\\&\times\left(|\mathbf{F}|^2-\frac{q_1}{1+q_1}|\mathbf{F}^{\mathrm{T}}\mathbf{n}_1|^2-\frac{q_2}{1+q_2}|\mathbf{F}^{\mathrm{T}}\mathbf{n}_2|^2\right)-3\Bigg)\\&+\Phi(q_1,q_2)+\frac{\alpha}{2}(|\mathbf{h}_1|^2+|\mathbf{h}_2|^2)\\&+\Gamma(q_1)K(\mathbf{F},\mathbf{n}_1,\mathbf{G}_1)+\Gamma(q_2)K(\mathbf{F},\mathbf{n}_2,\mathbf{G}_2).\end{aligned} \tag{3}$$

Here, $\mathbf{G}_\beta=\mathrm{Grad}\,\mathbf{n}_\beta$ is the gradient of the orientation $\mathbf{n}_\beta$; Φ is a quadruple-well potential, with local minima at $(q_1,q_2)=(0,0)$, $(q_1,q_2)=(0,q_*)$, $(q_1,q_2)=(q_*,0)$, and $(q_1,q_2)=(q_*,q_*)$, consistent with

$$\Phi(q_1,q_2)\to+\infty \quad \text{as} \quad q_1\to-1,+\infty \quad \text{or} \quad q_2\to-1,+\infty; \tag{4}$$

$\mathbf{h}_\beta=\mathrm{Grad}\,q_\beta$ is the gradient of the asphericity q_β; $\alpha>0$ is a *regularizing modulus*; Γ is a mollifying factor, dimensionless and consistent with

$$\begin{aligned}&\Gamma(q)=O(q^2) \quad \text{as} \quad q\to0,\\&\Gamma(q)>0 \quad \text{for} \quad q\neq0,\\&\Gamma(q)\to+\infty \quad \text{as} \quad q\to-1,+\infty;\end{aligned} \tag{5}$$

and K, involving *orientational-elasticity moduli* $\kappa_1>0$, $\kappa_2>0$, $\kappa_3>0$, $\kappa_4>0$, and $\kappa_5>0$, is a generalization of the energy density of the Oseen–Zöcher–Frank[5–7] (OZF) theory to account for deformation.

The first term of the right-hand side of (3) arises from (2) on taking $\mathbf{A}$ as given in (1) and $\boldsymbol{\Lambda}=\alpha\mathbf{1}$. The factor K appearing in the remaining terms on the right-hand side of (3) is of the form

$$\begin{aligned}K(\mathbf{F},\mathbf{n},\mathbf{G})=&\frac{\kappa_1}{2}(\mathbf{F}\cdot\mathbf{G})^2+\frac{\kappa_2}{2}|\mathbf{F}^{\mathrm{T}}\mathbf{G}|^2\\&+\frac{\kappa_3(|\mathbf{F}^{\mathrm{T}}\mathbf{G}\mathbf{F}^{\mathrm{T}}\mathbf{n}|^2+|\mathbf{G}^{\mathrm{T}}\mathbf{F}\mathbf{F}^{\mathrm{T}}\mathbf{n}|^2)}{2|\mathbf{F}^{\mathrm{T}}\mathbf{n}|^2}\\&+\frac{\kappa_4}{2}(\mathbf{F}^{\mathrm{T}}\mathbf{G})\cdot(\mathbf{G}^{\mathrm{T}}\mathbf{F})\\&+\frac{\kappa_5(\mathbf{F}^{\mathrm{T}}\mathbf{G}\mathbf{F}^{\mathrm{T}}\mathbf{n})\cdot(\mathbf{G}^{\mathrm{T}}\mathbf{F}\mathbf{F}^{\mathrm{T}}\mathbf{n})}{2|\mathbf{F}^{\mathrm{T}}\mathbf{n}|^2}.\end{aligned} \tag{6}$$

On setting $\mathbf{F}=\mathbf{1}$ in (6), we may identify $\kappa_1+\kappa_2+\kappa_4$, κ_2, $\kappa_2+\kappa_3$, and $\kappa_2+\kappa_4$ with the classical splay, twist, bend, and saddle-splay moduli of the OZF theory; $\kappa_3+\kappa_5$ is an additional modulus that accounts for interactions between the distortion of the network and the orientation of the molecular conformation. By (4) and (5), both Φ and Γ penalize states in which the conformation becomes overly oblate or prolate about any axis.

Within our framework, a disclination in a nematic elastomer is a tubular neighborhood within which the asphericity vanishes and the orientation is undefined. The orientation gradient and, hence, K are therefore singular within such a neighborhood. The mollifying factor Γ appearing in the final two terms on the right-hand side of (3) is introduced to render integrable any such singularities.[8]

If we restrict attention to states in which the asphericity is uniaxial, so that, without loss of generality, $q_1 \equiv q \neq 0$, $q_2 \equiv 0$, $\mathbf{n}_1 \equiv \mathbf{n}$, and $\mathbf{n}_2$ is undefined, then the free-energy density (3) reduces to the expression considered earlier.[1–3]

Granted (3) and that external body forces are absent, the variationally based equilibrium equations of the theory are

$$\mathrm{Div}\left(\frac{\partial \psi}{\partial \mathbf{F}}\right) = \mathbf{F}^{-\mathsf{T}} \mathrm{Grad}\, p, \tag{7a}$$

$$\mathrm{Div}\left(\frac{\partial \psi}{\partial \mathbf{h}_1}\right) = \frac{\partial \psi}{\partial q_1}, \tag{7b}$$

$$\mathrm{Div}\left(\frac{\partial \psi}{\partial \mathbf{h}_2}\right) = \frac{\partial \psi}{\partial q_2}, \tag{7c}$$

$$\mathrm{Div}\left(\frac{\partial \psi}{\partial \mathbf{G}_1}\right) + \left(\frac{\partial \psi}{\partial \mathbf{G}_1} \cdot \mathbf{G}_1\right)\mathbf{n}_1 = \frac{\partial \psi}{\partial \mathbf{n}_1}, \tag{7d}$$

$$\mathrm{Div}\left(\frac{\partial \psi}{\partial \mathbf{G}_2}\right) + \left(\frac{\partial \psi}{\partial \mathbf{G}_2} \cdot \mathbf{G}_2\right)\mathbf{n}_2 = \frac{\partial \psi}{\partial \mathbf{n}_2}, \tag{7e}$$

where all differentiation of ψ is performed on the manifold associated with the constraints $\det \mathbf{F} = 1$ and $|\mathbf{n}_\beta| = 1$, $\beta = 1,2$, and where p denotes the pressure required to maintain the constraint $\det \mathbf{F} = 1$. While (7a) expresses conventional balance of force associated with $\mathbf{y}$, (7b), (7c), (7d), and (7e) express generalized force balances associated, respectively, with the additional kinematical degrees of freedom q_1, q_2, $\mathbf{n}_1$, and $\mathbf{n}_2$.

Following the approach taken in previous work,[1–3] we use the theory to investigate the presence of disclinations of strength $+1$ in a nematic-elastomeric specimen that, in the reference state, occupies the right circular cylinder

$$\mathcal{R} = \{\mathbf{x} = r\mathbf{e}_r + z\mathbf{e}_z : 0 \leqslant r < R, |z| < \infty\}, \tag{8}$$

with cylindrical coordinates (r, θ, z) and $\{\mathbf{e}_r, \mathbf{e}_\theta, \mathbf{e}_z\}$ the associated physical basis. In so doing, we assume that the lateral surface $\partial\mathcal{R} = \{\mathbf{x} : |\mathbf{x}| = R\}$ of the specimen is free of all tractions, viz.,

$$\left(\frac{\partial \psi}{\partial \mathbf{F}} - p\mathbf{F}^{-\mathsf{T}}\right)\Big|_{\partial\mathcal{R}} \mathbf{e}_r = \mathbf{0}, \tag{9a}$$

$$\left.\frac{\partial \psi}{\partial \mathbf{h}_\beta}\right|_{\partial\mathcal{R}} \cdot \mathbf{e}_r = 0, \quad \beta = 1,2, \tag{9b}$$

$$\left.\frac{\partial \psi}{\partial \mathbf{G}_\beta}\right|_{\partial\mathcal{R}} \mathbf{e}_r = \mathbf{0}, \quad \beta = 1,2. \tag{9c}$$

Consistent with the requirement that the deformation be isochoric, we stipulate that

$$\mathbf{y}(r, \theta, z) = \lambda r \mathbf{e}_r + \frac{z}{\lambda^2}\mathbf{e}_z \quad \text{with} \quad \lambda > 0. \tag{10}$$

The case of $0 < \lambda < 1$ corresponds to radial contraction coupled with axial extension of the cylinder, while that of $\lambda > 1$ is compatible with the cylinder expanding radially while contracting along its axis. From (10),

$$\mathbf{F}(r, \theta, z) = \lambda(\mathbf{1} - \mathbf{e}_z \otimes \mathbf{e}_z) + \frac{1}{\lambda^2}\mathbf{e}_z \otimes \mathbf{e}_z, \tag{11}$$

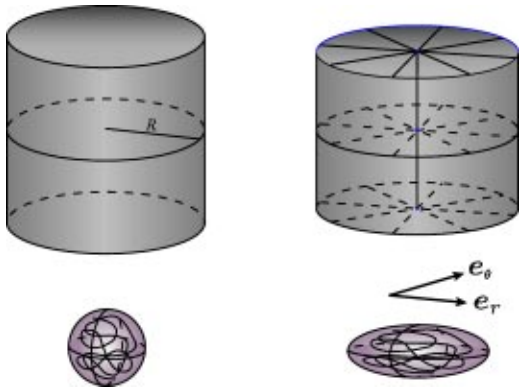

FIG. 1. Cylinder and molecular conformation in undistorted (a) and distorted (b) states.

and a direct calculation shows that, for all $\lambda > 0$, the constraint $\det \mathbf{F} = 1$ holds throughout $\mathcal{R}$. We emphasize that $\mathbf{F}$ is measured relative to the isotropic reference state. Figure 1 shows the specimen in its undistorted reference state and also in the deformed state.

When $q_\beta = 0$, the orientation $\mathbf{n}_\beta$ is undefined. When $q_1 \neq 0$, we assume that $\mathbf{n}_1$ is radial, so that

$$\mathbf{n}_1 = \mathbf{e}_r. \tag{12}$$

Further, when $q_2 \neq 0$, we suppose that $\mathbf{n}_2$ is azimuthal, so that

$$\mathbf{n}_2 = \mathbf{e}_\theta. \tag{13}$$

As a consequence of these choices, the constraint $|\mathbf{n}_\beta| = 1$ is satisfied whenever $\mathbf{n}_\beta$ is defined. A direct calculation shows that, when $\mathbf{n}_1$ and $\mathbf{n}_2$ are defined,

$$\begin{aligned} \mathbf{G}_1(r, \theta, z) &= \frac{1}{r}\mathbf{e}_\theta \otimes \mathbf{e}_\theta, \\ \mathbf{G}_2(r, \theta, z) &= -\frac{1}{r}\mathbf{e}_r \otimes \mathbf{e}_\theta. \end{aligned} \tag{14}$$

Further, we suppose that the asphericities q_1 and q_2 depend at most on the radial coordinate r.

Using (6) and (11)–(14) gives

$$\begin{aligned} K(\mathbf{F}, \mathbf{n}_1, \mathbf{G}_1) &= \frac{\kappa_{\mathrm{I}} \lambda^2}{2r^2}, \\ K(\mathbf{F}, \mathbf{n}_2, \mathbf{G}_2) &= \frac{\kappa_{\mathrm{II}} \lambda^2}{2r^2}, \end{aligned} \tag{15}$$

with $\kappa_{\mathrm{I}} = \kappa_1 + \kappa_2 + \kappa_4$ the *orientational splay modulus* and $\kappa_{\mathrm{II}} = \kappa_2 + \kappa_3$ the *orientational bend modulus*.

Since the deformation is prescribed via (10) and the orientations are either given as in (12) and (13) or undefined, the only unknowns are the pressure p and asphericities q_1 and q_2. From the radial component of (7a) and the assumption that q_1 and q_2 depend at most on r, it follows that p also may depend at most on r.

Letting ν be a parameter associated with the characteristic strength of the potential Φ and introducing $x = r/R$, $P(x) = p(Rx)/\nu$, and $Q_\beta(x) = q_\beta(Rx)$, $\beta = 1,2$, we obtain the dimensionless groups

$$\mu^*=\frac{\mu}{\nu},\quad \kappa_{\mathrm{I}}^*=\frac{\kappa_{\mathrm{I}}}{R^2\nu},\quad \kappa_{\mathrm{II}}^*=\frac{\kappa_{\mathrm{II}}}{R^2\nu},\quad \text{and}\ \ \alpha^*=\frac{\alpha}{R^2\nu}. \tag{16}$$

Using the radial components of (7a) and (9a), we find that the dimensionless pressure P has the form

$$P=\lambda^2\left(\mu^*\frac{(1+Q_2)^{1/3}}{(1+Q_1)^{2/3}}+\frac{\kappa_{\mathrm{II}}^*\Gamma(Q_2)}{x^2}+\mu^*I_1+I_2\right), \tag{17}$$

with

$$\begin{aligned} I_1(x)&=\int_x^1\frac{(Q_1(\xi)-Q_2(\xi))\,d\xi}{\xi(1+Q_1(\xi))^{2/3}(1+Q_2(\xi))^{2/3}},\\ I_2(x)&=\int_x^1\frac{(\kappa_{\mathrm{I}}^*\Gamma(Q_1(\xi))-\kappa_{\mathrm{II}}^*\Gamma(Q_2(\xi)))\,d\xi}{\xi^3}. \end{aligned} \tag{18}$$

From (7b) and (7c), we obtain the differential equations

$$\begin{aligned} &\frac{\alpha^*}{x}\frac{d}{dx}\left(x\frac{dQ_1}{dx}\right)\\ &\quad=\frac{\mu^*\lambda^2(1+Q_2)^{1/3}}{6(1+Q_1)^{2/3}}\left(\frac{1}{\lambda^6}-\frac{1-Q_1}{1+Q_1}-\frac{Q_2}{1+Q_2}\right)\\ &\qquad+\frac{\kappa_{\mathrm{I}}^*\lambda^2\Gamma'(Q_1)}{2x^2}+\frac{1}{\nu}\frac{\partial\Phi(Q_1,Q_2)}{\partial Q_1},\\ &\frac{\alpha^*}{x}\frac{d}{dx}\left(x\frac{dQ_2}{dx}\right)\\ &\quad=\frac{\mu^*\lambda^2(1+Q_1)^{1/3}}{6(1+Q_2)^{2/3}}\left(\frac{1}{\lambda^6}-\frac{Q_1}{1+Q_1}-\frac{1-Q_2}{1+Q_2}\right)\\ &\qquad+\frac{\kappa_{\mathrm{II}}^*\lambda^2\Gamma'(Q_2)}{2x^2}+\frac{1}{\nu}\frac{\partial\Phi(Q_1,Q_2)}{\partial Q_2}, \end{aligned} \tag{19}$$

which are augmented by the boundary conditions

$$\left.\frac{dQ_\beta}{dx}\right|_{x=0}=0\quad\text{and}\quad\left.\frac{dQ_\beta}{dx}\right|_{x=1}=0, \tag{20}$$

arising, respectively, from the assumed radial symmetry of the solution and (9b).

When $q_1=0$ and $\mathbf{n}_1$ is undefined, (7d) is vacuous. However, when $q_1\neq 0$ and $\mathbf{n}_1$ is therefore defined, direct calculations show that (7d) is satisfied. Entirely analogous remarks hold concerning q_2, $\mathbf{n}_2$, and (7e). For $\mathbf{n}_1$ and $\mathbf{n}_2$ as defined in (12) and (13), the boundary conditions (9c) are satisfied.

III. NUMERICAL RESULTS

The differential equation (19) involves functions Φ and γ, which are restricted only by (4) and (5). Although many function choices would satisfy these restrictions, for consistency and ease of comparison with the results for the uniaxial case,[1–3] for our numerical investigations we chose forms for Φ and Γ similar to those used in our previous work, viz.,

$$\Phi(q_1,q_2)=\frac{\nu q_1^2(q_1-q_*)^2}{2(1+q_1)^2}+\frac{\nu q_2^2(q_2-q_*)^2}{2(1+q_2)^2} \tag{21}$$

and

$$\Gamma(q)=\begin{cases}\dfrac{q^2}{(1+q)^2} & \text{if}\ \ -1<q\leqslant 0,\\ q^2 & \text{if}\ \ q\geqslant 0.\end{cases} \tag{22}$$

The particular choice (21) of Φ obeys $\Phi(q_1,q_2)=\Phi(q_2,q_1)$. This symmetry allows either of the axes $\mathbf{n}_1=\mathbf{e}_r$ or $\mathbf{n}_1=\mathbf{e}_\theta$ to serve as the primary director. A consequence of this property is that both the isotropic-uniaxial and isotropic-biaxial transitions are of first order. Although the uniaxial–biaxial transition in conventional liquid crystals is normally of second order, a direct, first-order isotropic-biaxial transition has been recognized and can occur.[9] Furthermore, in contrast to traditional liquid crystals, the rubberlike nature of nematic elastomers allows them to sustain a first-order transition between uniaxial and biaxial states.[10] Thus, we envison a direct first-order transition between the isotropic and biaxial states as feasible. In addition, (21) is such that $\Phi(0,q_2)=\Phi(q_*,q_2)=0$ [and, since $\Phi(q_1,q_2)=\Phi(q_2,q_1)$, $\Phi(q_1,0)=\Phi(q_2,q_*)=0$]. This property renders the isotropic and nematic states equally favorable and, thus, is valid only at the nematic–isotropic transition temperature. Thus, our predictions are confined to a narrow range of temperatures about the nematic–isotropic transition temperature. Alternative forms for Φ that relax both the symmetry $\Phi(q_1,q_2)=\Phi(q_2,q_1)$ and the assumed equal preference for the isotropic and nematic states would yield a theory capable of accounting for the possibly second-order nature of uniaxial–biaxial transitions and for behavior away from the nematic-isotropic transition temperature. Such alternatives would require the consideration of additional temperature-dependent material parameters to describe, for instance, the relative heights of the various potential wells. For this reason, we leave the study of such alternatives to future work. While defined piecewise, the particular choice (22) of Γ is twice continuously-differentiable. Since the differential equations in (19) involve only the first derivative of Γ, we therefore expect no numerical difficulties to ensue from this choice.

To solve the boundary-value problem (19)–(20) numerically, we incorporated (21) and (22) and selected parameters as follows: As before,[1–3] we chose $\mu=10^5$ J/m^3, $\nu=10^6$ J/m^3, and $R=1$ cm. Underlying the chosen value of ν is the notion that, whereas μ should scale like $k_B\theta$ per polymer chain, with k_B Boltzmann's constant and θ the absolute temperature, ν should scale like $k_B\theta$ per monomer. To attain the high extensibilities associated with rubberlike behavior requires upwards of 15–100 monomers per chain, whereby ν should exceed μ by at least an order of magnitude. For traditional nematics at temperatures in a wide range below the clearing temperature, the bend modulus κ_{II} is on the order of 10^{-12} J/m and is three-halves to two times the splay modulus κ_{I}.[11–14] The values of these moduli have not yet been determined for nematic elastomers, but, because of the rubbery nature of these materials, it seems reasonable to expect that the moduli would be at least an order of magnitude greater.[15] So, we took $\kappa_{\mathrm{I}}=10^{-11}$ J/m and $\kappa_{\mathrm{II}}=2\times10^{-11}$ J/m. The value of the splay modulus is also in line with values used in previous work.[1–3,15,16] With the expectation that the regularizing modulus should not exceed the splay modulus, we

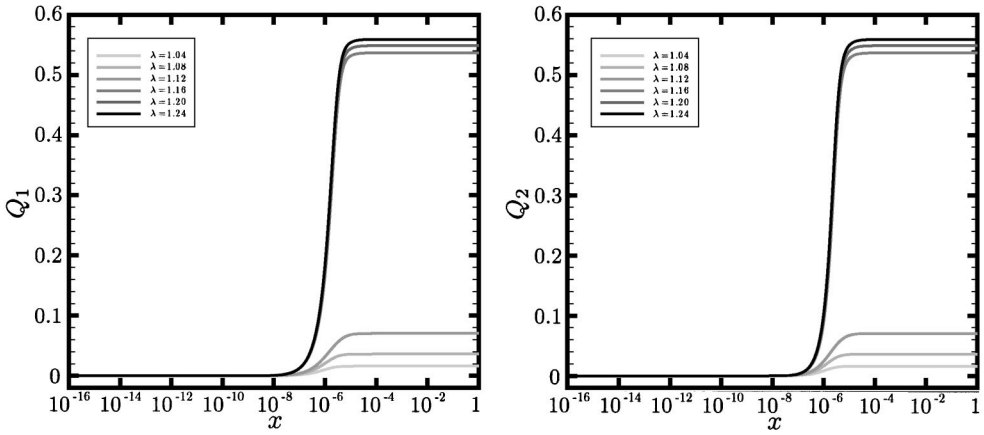

FIG. 2. Plots of the asphericities Q_1 and Q_2 as functions of dimensionless radial position x (note logarithmic scale) for the dimensionless material parameters $\mu^*=0.1$, $\kappa_{\mathrm{I}}^*=\frac{1}{2}\kappa_{\mathrm{II}}^*=\alpha^*=10^{-13}$, and $q_*=0.5$ and representative values of the degree of radial expansion λ between 1 and 1.25. Consistent with (20), note the horizontal slopes at the cylinder center ($x=0$) and outer boundary ($x=1$).

chose $\alpha=10^{-11}$. As a result of the foregoing assumptions, $\mu^*=10^{-1}$ and $\kappa_{\mathrm{I}}^*=\frac{1}{2}\kappa_{\mathrm{II}}^*=\alpha^*=10^{-13}$. Although our chosen value of ν is quite small, a larger and, thus, more realistic value would lead to smaller values of κ_{I}^*, κ_{II}^*, and α^* and thus make the singularly perturbed boundary-value problem (19) and (20) more computationally intensive to solve. Since radial expansion ($\lambda>1$) is expected to give rise to prolate asphericities ($q_1>0$ and perhaps $q_2>0$ as well) perpendicular to the cylinder axis, the choice $q_*>0$ is sensible for this case. Similarly, because we expect oblate asphericities ($-1<q_1<0$ and perhaps $q_2<0$ too) perpendicular to the axis to arise for radial contraction ($0<\lambda<1$), we choose $-1<q_*<0$ in this setting. So, for illustrative purposes, we took $q_*=0.5$ for radial expansion and $q_*=-0.4$ for radial contraction.

With these parameters, we solved (19) and (20) from $x=0$ to $x=1$ using the ACDC package[17] with the tolerance on the solution pair (Q_1,Q_2) set to 10^{-8} and that of its derivative $(dQ_1/dx, dQ_2/dx)$ set to 10^{-4} for radial expansion and 10^{-3} for radial contraction. As a trial solution, we used the straight line $Q_1=Q_2=0$, satisfying (20) and consisting of 5001 evenly spaced points on the closed domain. The only parameter varied was λ, the degree of radial expansion or contraction. Thus, the range of λ for axial contraction; the values of μ^*, ν, κ_{I}^*, and α^*; and the solution method were identical to those used in our previous investigations.[1–3]

A. Radial expansion ($\lambda>1$)

For the regime of radial expansion, we allowed λ to range between 1 and 1.25. Figure 2 shows the solution profiles for Q_1 and Q_2 and the sharp transition between isotropic ($Q_\beta=0$, $\beta=1,2$) and anisotropic ($Q_\beta\neq 0$) regions along the cylinder radius, thereby indicating the presence of a disclination of strength $+1$ located along the cylinder axis. The extent of the disclination core can also be inferred from the plot as the region where Q_1 and Q_2 exhibit rapid increases.[18] Although the solutions for Q_1 and Q_2 appear identical in Fig. 2, it becomes apparent in Fig. 3 that they differ but only in the core region, where Q_2 exhibits an increased gradient due to the larger value of κ_{II} compared to κ_{I}. (For clarity, Fig. 3 focuses on $\lambda=1.20$; but similar behavior is evident for the studied range of λ.) Despite this difference, from Fig. 2, the transition zones for Q_1 and Q_2 both appear to be centered at $x=10^{-6}$, corresponding to a dimensional core radius on the order of 10^{-2} μm and consistent with the length scale predicted by the ratios $\sqrt{\kappa_{\mathrm{I}}/\mu}$ and $\sqrt{\kappa_{\mathrm{II}}/\mu}$ for our choices of μ, κ_{I}, and κ_{II}. The ratios $\sqrt{\kappa_{\mathrm{I}}/\mu}$ and $\sqrt{\kappa_{\mathrm{II}}/\mu}$ determine the length scale at which a crossover between rubber-elastic and orientational effects occurs.[19–21] Our core radius, which we denote by x_c, is also of the same order as values observed for liquid crystalline melts.[22] Since our uniaxial energy density investigations resulted in disclinations with similar characteristics,[1–3] these results are not unexpected. What is important to emphasize is that, since both Q_1 and Q_2 are nonvanishing for $x>x_c$, the states obtained here are *biaxial*.

To investigate the energetic status of these biaxial states, we introduce the dimensionless free-energy density $\Psi=\psi/\nu$. In view of the assumptions concerning the deformation **y**, the orientations $\mathbf{n}_1$ and $\mathbf{n}_2$, and the asphericities q_1 and q_2,

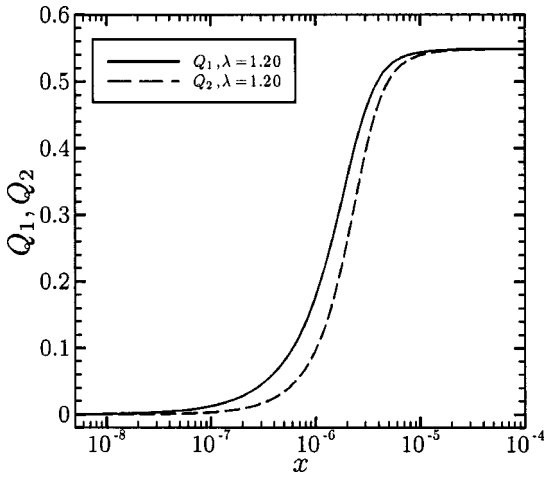

FIG. 3. Plot of the asphericities Q_1 and Q_2 in the core region as a function of dimensionless radial position x (note logarithmic scale) for the degree of radial expansion $\lambda=1.20$ and the dimensionless material parameters $\mu^*=0.1$, $\kappa_{\mathrm{I}}^*=\frac{1}{2}\kappa_{\mathrm{II}}^*=\alpha^*=10^{-13}$, and $q_*=0.5$.

$$\Psi = \frac{\psi}{\nu} = \Psi_e + \Psi_a + \Psi_o, \tag{23}$$

with

$$\Psi_e = \frac{\mu^*}{2}\left(2\lambda^2 + \frac{1}{\lambda^4} - 3\right) \tag{24}$$

a conventional neo-Hookean rubber-elastic contribution associated with the distortion of the network,

$$\Psi_a = \frac{\mu^*}{2}\left(\lambda^2\left(\frac{(1+Q_2)^{1/3}}{(1+Q_1)^{2/3}} + \frac{(1+Q_1)^{1/3}}{(1+Q_2)^{2/3}} - 2\right) + \frac{1}{\lambda^4}((1+Q_1)^{1/3}(1+Q_2)^{1/3} - 1)\right) + \frac{\Phi(Q_1,Q_2)}{\nu} + \frac{\alpha^*}{2}\left(\left(\frac{dQ_1}{dx}\right)^2 + \left(\frac{dQ_2}{dx}\right)^2\right) \tag{25}$$

a contribution associated with the asphericity of the molecular conformation, and

$$\Psi_o = \frac{(\kappa_{\mathrm{I}}^* + \kappa_{\mathrm{II}}^*)\lambda^2 \Gamma(Q_1,Q_2)}{2x^2} \tag{26}$$

a contribution associated with the axes of the molecular conformation.

A comparision of the total neo-Hookean energy

$$\mathcal{F}_e^{\mathrm{tot}} = \int_0^1 \Psi_e(x)\, x\, dx, \tag{27}$$

the total energy from our previously performed uniaxial investigations $\mathcal{F}_{\mathrm{uni}}^{\mathrm{tot}}$,[1–3] and the total free energy

$$\mathcal{F}^{\mathrm{tot}} = \int_0^1 \Psi(x)\, x\, dx \tag{28}$$

plotted in Fig. 4(a) shows that the material strongly prefers a disclinated state in which the conformation of the material surrounding the core is biaxial as opposed to uniaxial. While $\mathcal{F}_e^{\mathrm{tot}}$ increases monotonically with λ, $\mathcal{F}^{\mathrm{tot}}$ is a double-well potential with an absolute minimum at $\lambda = 1$ and a relative minimum at $\lambda \approx 1.13$. Also, for all $\lambda > 1$, $\mathcal{F}^{\mathrm{tot}}$ is less than both $\mathcal{F}_{\mathrm{uni}}^{\mathrm{tot}}$ and $\mathcal{F}_e^{\mathrm{tot}}$, the isotropic ($Q_1 = Q_2 = 0$) neo-Hookean contribution alone. This difference is negligible for all $\lambda \leqslant 1.12$, and we therefore do not necessarily expect a disclinated state to form in the range $1 \leqslant \lambda < 1.12$. However, beyond $\lambda = 1.12$, the difference between $\mathcal{F}^{\mathrm{tot}}$ and $\mathcal{F}_e^{\mathrm{tot}}$ becomes nontrivial and shows an energetic motivation for the material to form a disclinated state in which the material outside the core boundary x_c in a biaxially anisotropic state. It is interesting to note from Fig. 4(a) that not only is a biaxial state energetically preferred over a uniaxial one ($\mathcal{F}^{\mathrm{tot}}$ always falls below $\mathcal{F}_{\mathrm{uni}}^{\mathrm{tot}}$ for our range of λ) but also that the threshold value of λ at which a biaxial disclination first manifests itself is less than that arising when the extra-core region is constrained to be uniaxial.

In addition, we investigated the total free energy of the core, which we denote as

$$\mathcal{F}^{\mathrm{core}} = \int_0^{x_c} \Psi(x)\, x\, dx, \tag{29}$$

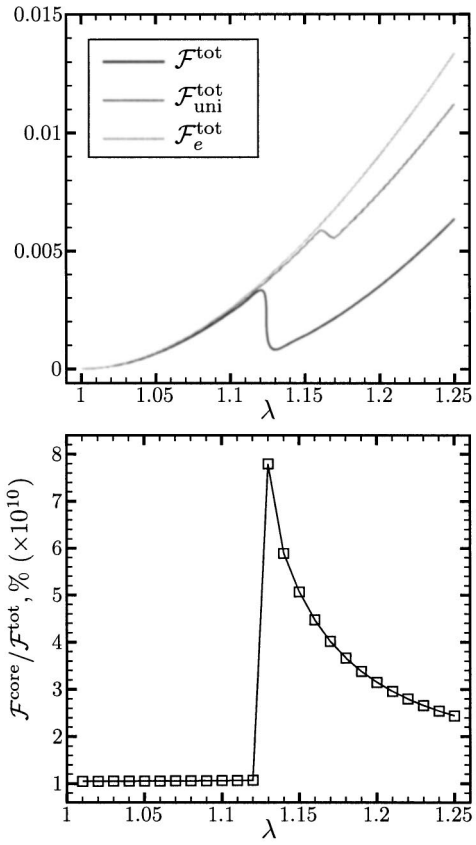

FIG. 4. (a) Plots of the total neo-Hookean rubber-elastic energy $\mathcal{F}_e^{\mathrm{tot}}$ and of the total free-energy $\mathcal{F}^{\mathrm{tot}}$ as a function of the degree of radial expansion λ between 1 and 1.25 for the dimensionless material parameters $\mu^* = 0.1$, $\kappa_{\mathrm{I}}^* = \frac{1}{2}\kappa_{\mathrm{II}}^* = \alpha^* = 10^{-13}$, and $q_* = 0.5$. (b) Plot of the percentage $\mathcal{F}^{\mathrm{core}}/\mathcal{F}^{\mathrm{tot}}$ of free energy in the core as a function of the degree of cylinder distortion λ between 1 and 1.25 for the dimensionless material parameters $\mu^* = 0.1$, $\kappa_{\mathrm{I}}^* = \frac{1}{2}\kappa_{\mathrm{II}}^* = \alpha^* = 10^{-13}$, and $q_* = 0.5$.

relative to that of the whole domain. From Fig. 4(b), it is evident that $\mathcal{F}^{\mathrm{core}}$ is a vanishingly small percentage of $\mathcal{F}^{\mathrm{tot}}$. This is because of the relatively small size of the core and the fact that Ψ_e is of a comparatively large magnitude across the entire radial extent of the cylinder. As in our previous studies,[1–3] the proportion of total free-energy contained in the core remains relatively constant up to the value of λ corresponding to the first inflection point of $\mathcal{F}^{\mathrm{tot}}$. Coincident with the threshold value of λ seen in Fig. 4(a), a sharp increase then occurs, and the proportion then decreases monotonically for the remainder of our range as more energy goes into both stretching of the polymer network and changing the conformation of the chains comprising the network.

The dimensionless pressure P given in (17) is shown in Fig. 5(b). Because the material becomes biaxial with $Q_1 \neq 0$ and $Q_2 \neq 0$, the pressure differs both in magnitude and character from that arising in the uniaxial case.[1–3] Because $Q_1 = Q_2$ except within the transition layer, the term $I_1(x)$ in (17) vanishes everywhere but within the layer. In the isotropic core, where $Q_1 = Q_2 = 0$, the pressure coincides with its neo-Hookean counterpart and is an order of magnitude lower than in the uniaxial case.[1–3] Outside the core, with the increase in both Q_1 and Q_2 shown in Fig. 2, the pressure drops below the neo-Hookean value. Recall that, for an incom-

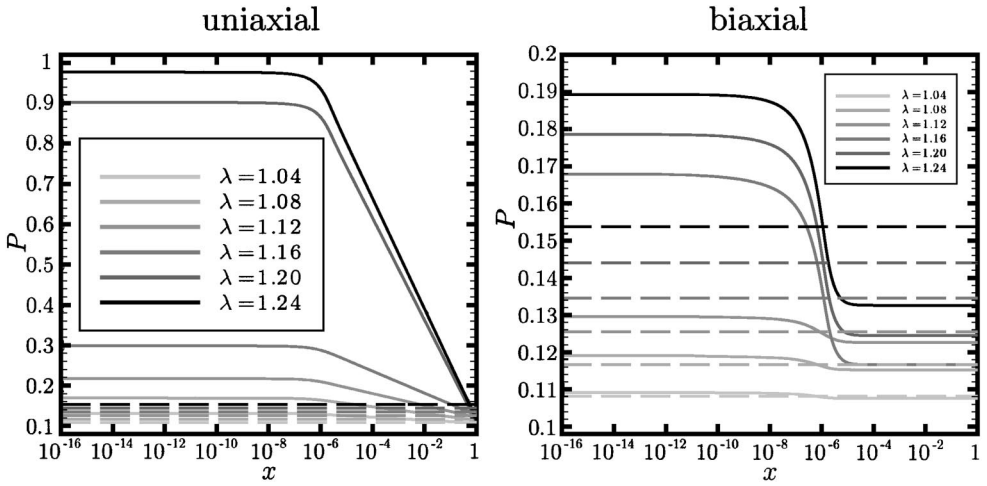

FIG. 5. Plot of the dimensionless pressure P for the (a) uniaxial case (Ref. 2) and (b) biaxial case as a function of dimensionless radial position x (note logarithmic scale) for the dimensionless material parameters $\mu^*=0.1$, $\kappa_{\mathrm{I}}^*=\frac{1}{2}\kappa_{\mathrm{II}}^*=\alpha^*=10^{-13}$, and $q_*=0.5$ and representative values of the degree of radial expansion λ between 1 and 1.25. Dashed lines show corresponding neo-Hookean values of P.

pressible material, the pressure is a reaction which arises in response to the constraint $\det \mathbf{F}=1$. The excessive core pressure found in the uniaxial case, which general exceeds its biaxial counterpart by an order of magnitude, indicates that the material is overly constrained when it is forced to remain incompressible and biaxial conformations are disallowed. When biaxial conformations are allowed, there is a concomitant decrease in the reactive pressure and that decrease further confirms the preference of the material for a biaxial state.

B. Radial contraction (0<λ<1)

The analogous problem of axial extension was investigated with a range of λ between 1 and 0.80. As in the case of axial contraction, plots of the asphericities Q_1 and Q_2 show sharp transitions between isotropic ($Q_1=Q_2=0$) and anisotropic ($Q_1=Q_2\neq 0$) regions along the cylinder radius, consistent with the presence of a biaxial disclination of strength $+1$ located along the cylinder axis. Figure 6 shows the solution profile for Q_1. As in the case of axial contraction, Q_1 and Q_2 are equal except in the transition region separating the core and extra-core; in that transition region, Q_2 exhibits a steeper gradient due to the larger value of κ_{II} compared to κ_{I}. Also, the transition zones for Q_1 and Q_2 both appear to be at $x=10^{-6}$, corresponding as before to a dimensional core radius on the order of 10^{-2} μm.

The energies $\mathcal{F}_e^{\mathrm{tot}}$, $\mathcal{F}_{\mathrm{uni}}^{\mathrm{tot}}$, $\mathcal{F}^{\mathrm{tot}}$ for radial contraction are plotted in Fig. 7. Here too, as for radial expansion, there is an energetic motivation for the material to achieve a biaxial disclinated state, especially for $\lambda<0.92$. This threshold value of λ occurs sooner; i.e., at a lesser degree of radial contraction, than for the corresponding uniaxial case.

The behavior of the total free energy $\mathcal{F}^{\mathrm{core}}$ of the core is similar to that observed for axial contraction. The proportion of total free energy contained in the core remains relatively constant up to the value of λ corresponding to the first inflection point of $\mathcal{F}^{\mathrm{tot}}$. As before, coincident with the threshold value of λ of the total free energy in Fig. 7, a sharp increase then occurs, and the proportion then decreases monotonically for the rest of the range.

As in the case of radial expansion, a determination of the pressure from (17) can be made. These results are omitted here for brevity.

IV. BIFURCATION AND STABILITY

A priori, the uniqueness and stability of the numerical solutions discussed in Sec. III are unclear. To address these issues, we examine the solution set for the boundary-value problem (19) and (20) for scalings where κ_{I}^*, κ_{II}^*, and α^* are all very small in comparison to μ^*. For brevity, we discuss only the case of radial expansion. The results for radial contraction are entirely analogous.

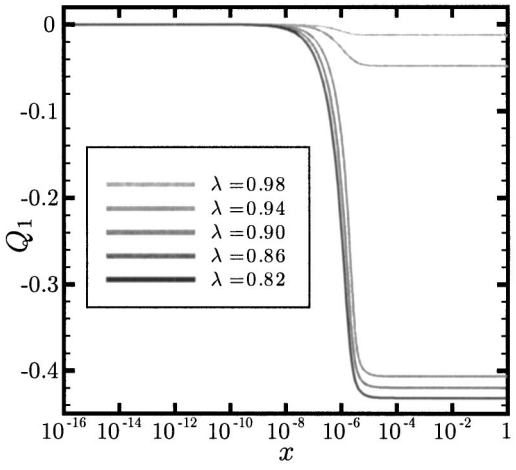

FIG. 6. Plots of the asphericity Q_1 as a function of dimensionless radial position x (note logarithmic scale) for the dimensionless material parameters $\mu^*=0.1$, $\kappa_{\mathrm{I}}^*=\frac{1}{2}\kappa_{\mathrm{II}}^*=\alpha^*=10^{-13}$, and $q_*=-0.4$ and representative values of the degree of axial expansion λ between 1 and 0.80. Consistent with (20), note the horizontal slopes at the cylinder center ($x=0$) and outer boundary ($x=1$). The analogous plots for Q_2 are indistinguishible from those for Q_1 except within the transition layer.

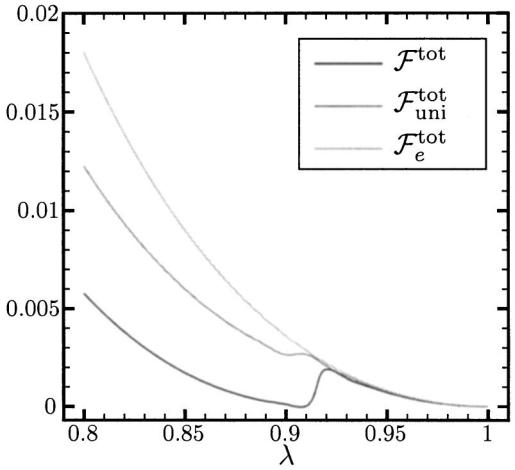

FIG. 7. Plots of the total neo-Hookean rubber-elastic energy $\mathcal{F}_e^{\rm tot}$ and of the total free-energy $\mathcal{F}^{\rm tot}$ as a function of the degree of axial expansion λ between 1 and 0.80 for the dimensionless material parameters $\mu^*=0.1$, $\kappa_{\rm I}^*=\frac{1}{2}\kappa_{\rm II}^*=\alpha^*=10^{-13}$, and $q_*=-0.4$.

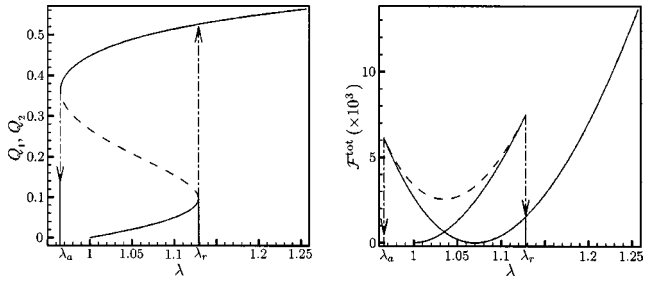

FIG. 8. (a) Plot of the constant, bulk asphericity Q as a function of the degree of radial expansion λ between 1 and 1.25 for the dimensionless material parameters $\mu^*=0.1$ and $q_*=0.5$. The equilibrium set consists of two (lower and upper) stable branches, and one (middle) unstable branch. When a certain deformation of $\lambda_r\approx 1.13$ is reached, the solution switches from the lower to the upper branch, with a sharp increase in Q (cf. Fig. 2). A classical hysteresis loop is present. (b) Plot of the total free-energy of the constant, bulk asphericity Q as a function of the degree of radial expansion λ between 1 and 1.25 for the dimensionless material parameters $\mu^*=0.1$ and $q_*=0.5$ (cf. Fig. 2). We observe two, stable (solid) branches connected by an unstable (dashed) one. Corresponding branch switching is highlighted by arrows and always leads to a lowering of the total free-energy.

Considering the structure of (19) and the numerical results depicted in Fig. 2, we conclude that for each $\lambda\neq 1$, the profiles of the solution pair (Q_1,Q_2) exhibit three well-defined regions:

(i) a core region surrounding the cylinder axis where (Q_1,Q_2) is uniform and very close to zero;
(ii) an extra-core region within which (Q_1,Q_2) is uniform but nonvanishing;
(iii) a transition layer connecting the core and extra-core regions.

Granted the scaling considered here, the dimensionless core region is both very thin, with width on the order of 10^{-6} (cf. Fig. 3), and energetically insignificant since its share of the free energy is never more than a minute percentage of the total [cf. Fig. 4(a)]. The structure of the transition layer is the same for all relevant λ; it monotonically connects $Q_1=Q_2=0$ at $x=0$ to the value of $Q_1=Q_2\neq 0$ in the extra-core region. We thus focus on the extra-core regime where symmetric behavior prevails in the sense that $Q_1=Q_2=Q$. A breakdown of this symmetry occurs only when the full domain is taken into account as in the preceding section. Neglecting the small parameters α^*, $\kappa_{\rm I}^*$, and $\kappa_{\rm II}^*$ associated with the core boundary, we specialize (19) to the extra-core region. This yields the algebraic equation,

$$f(Q,\lambda)=\frac{\mu^*\lambda^2}{6(1+Q)^{1/3}}\left(-\frac{1}{1+Q}+\frac{1}{\lambda^6}\right)+\frac{Q(Q-Q_*)(Q^2+2Q-Q_*)}{(1+Q)^3}=0, \qquad (30)$$

that should provide the uniform, common value Q of Q_1 and Q_2 outside the core. To predict the response of the material to any particular choice of λ, we would like to solve (30) for Q as a function of λ. Unfortunately, (30) contains fractional powers of Q and does not easily lend itself to direct analytical solution. To circumvent this obstacle, we note that (30) can be expressed as a cubic for λ^2, viz.,

$$\lambda^6+3b\lambda^4+c=0,$$

where

$$b=-\frac{2Q(Q-Q_*)(Q^2+2Q-Q_*)}{\mu^*(1+Q)^{5/3}}$$

and

$$c=-(1+Q).$$

Solving this equation yields

$$\lambda=\sqrt{b+s_-(b,c)+s_+(b,c)},$$

with

$$s_\pm(b,c)=-\left(\frac{b^2}{3}+\frac{c}{2}\pm\sqrt{\frac{b^3c}{3}+\frac{c^2}{4}}\right)^{1/3}.$$

A real value of λ is guaranteed by the range of parameters under consideration.

Having obtained $\lambda=\lambda(Q)$, we determine the originally desired function $Q=Q(\lambda)$ by plotting a bifurcation diagram [Fig. 8(a)] for (30). This provides substantial insight into the results obtained by direct numerical solution of the governing boundary-value problem (19) and (20) and shown in Fig. 2. We start from the point $(\lambda,Q)=(1,0)$ in Fig. 8(a), gradually increase the value of λ, and follow the lower branch of the diagram up to $\lambda=\lambda_r$. Above λ_r, the equilibrium solution for Q_1 and Q_2 is forced to switch to the upper branch (cf. Fig. 2). If we instead start on the upper branch at $\lambda>\lambda_r$ and quasistatically release the cylinder (decrease λ), we follow the upper branch past λ_r all the way down to a point of downward snapping, where $\lambda=\lambda_a<\lambda_r$. For this to occur, we must actually contact the specimen radially since $\lambda_a\leqslant 1$. Therefore, classical hysteretic behavior is observed.

To further clarify properties of the system, we can investigate the stability of solutions using the information about their behavior in the extra-core region obtained above. Since the bifurcation behavior observed in Fig. 8(a) is classical, the branch stability is as shown. In the same vein, we plot the

free energy of the constant, bulk solution in Fig. 8(b). We note that the sharp changes in free energy shown in Fig. 4 for radial expansion mirror the branch stability switching phenomenon described above. As can be seen, switching leads to a lower free energy level, and thus is preferable.

To determine the values of λ_r and λ_a in Fig. 8, we first note from (30) that $f(Q,\lambda)=0$ everywhere on both curves. Thus,

$$\frac{df}{dQ}=\frac{\partial f}{\partial Q}+\frac{\partial f}{\partial \lambda}\frac{\partial \lambda}{\partial Q}=0.$$

For λ_r and λ_a, this is supplemented by the fact that $\partial\lambda/\partial Q=0$. If $\partial f/\partial\lambda\neq 0$, then for the above equation to hold, $\partial f/\partial Q=0$. Therefore, λ_r and λ_a can be found by solving the system $(f(Q,\lambda),\partial f(Q,\lambda)/\partial Q)=(0,0)$. This gives rise to

$$\begin{aligned}&8(-2Q^2(9+Q(7+2Q))+Q(18+Q(3+Q))Q_*\\&\quad+(-3+5Q)Q_*^2)^2(7Q^4-4Q^3(-5+Q_*)\\&\quad+3Q_*^2-2QQ_*(9+Q_*)-6Q^2(-3+2Q_*))\\&\quad+(1+Q)^6(\mu^*)^3=0\end{aligned}\tag{31}$$

and

$$\lambda^2=-\frac{2(18Q^2+12Q^3+3Q^4+Q(Q-Q_*)(Q(2+Q)-Q_*)+3Q_*^2-6QQ_*(3+Q_*))}{(1+Q)^{5/3}\mu^*}.\tag{32}$$

Real solutions to (31) and (32) are not guaranteed and depend on the values of the parameters μ^* and Q_*. For the case of radial expansion, $(Q,\lambda_r)=(0.097,1.13)$ and $(Q,\lambda_a)=(0.36,0.97)$. These two values of λ_r, respectively, correspond to the point at which jumps are observed in Fig. 4. If a nematic-elastomeric specimen is being prepared for an experiment, (31) and (32) can be solved with the particular μ^* and Q_* being considered to see whether real λ_a and λ_r exist and, if so, what their values are. This then gives the experimentalist an idea of the range of axial contraction or extension to investigate.

The stability analysis described above is predicated on neglecting the parameters α^*, κ_{I}^*, and κ_{II}^* associated with the core boundary in (19) and which are small relative to μ^*. The question therefore arises as to how small α^*, κ_{I}^*, and κ_{II}^* must be to safely ignore them in the extra-core region. Thus, for a given λ, below a certain threshold and regardless of their values, α^*, κ_{I}^*, and κ_{II}^* should affect only the core boundary region of the solution (Q_1,Q_2) with the extra-core and core regions maintaining constant values. Keeping μ^* constant while changing the other parameters requires changing the specimen radius R. So, if the small parameters are below the threshold for constant (Q_1,Q_2), and since $\Psi=\Psi(Q_1,Q_2)$ [cf. (23)–(26)], it follows that the total, dimensional energy $\mathcal{F}^{\mathrm{tot}}\nu R^2$ [cf. (28)] will grow as R^2.

For a representative value of $\lambda=1.20$, we conducted a parametric study wherein $\mu=10^5$ J/m^3, $\nu=10^6$ J/m^3, $q_*=0.5$, $\kappa_{\mathrm{I}}=10^{-11}$ J/m and $\kappa_{\mathrm{II}}^*=2\times10^{-11}$ J/m were kept constant as before and only R was varied from 3.18×10^{-9} m to 1 cm. As a result, $\mu^*=10^{-1}$ remained constant and $\kappa_{\mathrm{I}}^*=\frac{1}{2}\kappa_{\mathrm{II}}^*=\alpha^*$ varied with R from 0.99 to 1×10^{-13}. For $R\leqslant 3.43\times10^{-8}$ m, we found that $\mathcal{F}^{\mathrm{tot}}\nu R^2\propto R^2$. This is because both Q_1 and Q_2 lie below the threshold for a disclination to necessarily appear. For $R\geqslant 3.54\times10^{-8}$ m ($\alpha^*\leqslant 0.008$), a disclination is present, but for $R<3.16\times10^{-7}$ m ($\alpha^*>1\times10^{-4}$) we found that $\mathcal{F}^{\mathrm{tot}}\nu R^2\propto R^{1.6}$. Since $\mathcal{F}^{\mathrm{tot}}\nu R^2$ grows less than quadratically in this region, we expect that a disclination will be easier to generate in specimens with $3.54\times10^{-8}\leqslant R<3.16\times10^{-7}$ m ($1\times10^{-4}<\alpha^*\leqslant 0.008$). The growth is not quadratic because, for such values of R, Q_1 and Q_2 do not attain a constant extra-core value. As stated previously, once this constant value threshold has been attained for $R\geqslant 3.16\times10^{-7}$ m ($\alpha^*\leqslant 1\times10^{-4}$), the small parameters only affect behavior in the transition layer. Thus, if $R\geqslant 3.16\times10^{-7}$ m ($\alpha^*\leqslant 1\times10^{-4}$), $\mathcal{F}^{\mathrm{tot}}\nu R^2\propto R^2$ and we conclude that the small parameters can only be discarded for this regime.

V. DISCUSSION

We have extended a previously studied to allow for biaxiality of the molecular conformation. In so doing, we have found that nematic elastomers can sustain disclinations with an isotropic core and an extra-core region in which the conformation is biaxial rather than uniaxial. These states possess lower energies than the corresponding ones for materials whose conformations are constrained to remain uniaxial. Furthermore, when compared to both the uniaxial and neo-Hookean cases, the reactive pressure required to maintain the constraint of material incompressibility within the disclination core is reduced by an order of magnitude. Thus, a biaxial disclinated state is a more natural one for the material to inhabit. In addition, we have used bifurcation and stability analyses to expand our insight regarding the properties of the governing equations and confidence in the numerical results. These analyses include the derivation of analytic expressions for the threshold values of radial expansion and contraction at which a biaxial disclinated state clearly becomes energetically preferred and a determination of the stability of solutions for the studied parameter values. Finally, for a representative case of axial contraction, we find the threshold at which the small parameters only affect the core boundary region and thus cause the total dimensional energy to vary with R^2 as theoretically predicted. When the parameters exceed the threshold, the dimensional energy varies as $R^{1.6}$, and we infer that a disclination will form more easily in specimens in this regime.

ACKNOWLEDGMENTS

We thank Don Carlson for many valuable discussions. This work was supported by the National Science Foundation and the Department of Energy.

[1] E. Fried and R. E. Todres, Proc. Natl. Acad. Sci. U.S.A. **98**, 14773 (2001).
[2] E. Fried and R. E. Todres, J. Mech. Phys. Solids **50**, 2691 (2002).
[3] E. Fried and R. E. Todres, J. Polym. Sci., Part B: Polym. Phys. **40**, 2098 (2002).
[4] M. Warner, K. P. Gelling, and T. A. Vilgis, J. Chem. Phys. **88**, 4008 (1988).
[5] W. C. Oseen, Trans. Faraday Soc. **29**, 883 (1933).
[6] H. Zöcher, Trans. Faraday Soc. **29**, 945 (1933).
[7] F. C. Frank, Discuss. Faraday Soc. **250**, 19 (1958).
[8] J. L. Ericksen, Arch. Ration. Mech. Anal. **113**, 97 (1991).
[9] R. Alben, J. Chem. Phys. **59**, 4299 (1973).
[10] H. R. Brand and O. Müller, Macromol. Theory Simul. **11**, 154 (2002).
[11] I. Haller, J. Chem. Phys. **57**, 1400 (1972).
[12] J. D. Bunning, T. E. Faber, and P. L. Sherell, J. Phys. (Paris) **42**, 1175 (1981).
[13] M. J. Bradshaw, E. P. Raynes, J. D. Dunning, and T. E. Faber, J. Phys. (Paris) **46**, 1513 (1985).
[14] E. G. Virga, *Variational Theories for Liquid Crystals* (Chapman & Hall, London, 1994).
[15] J. Schmidtke, W. Stille, and G. Strobl, Macromolecules **33**, 2922 (2000).
[16] M. Warner and E. M. Terentjev, Prog. Polym. Sci. **21**, 853 (1996).
[17] J. R. Cash and R. W. Wright, Appl. Numer. Math. **28**, 227 (1988).
[18] N. J. Mottram and S. J. Hogan, Philos. Trans. R. Soc. London, Ser. A **355**, 2045 (1997).
[19] G. C. Verwey, M. Warner, and E. M. Terentjev, J. Phys. II **6**, 1273 (1996).
[20] H. Finkelmann, I. Kundler, E. M. Terentjev, and M. Warner, J. Phys. II **7**, 1059 (1997).
[21] E. Fried and V. Korchagin, Int. J. Solids Struct. **39**, 3451 (2002).
[22] S. Chandrasekhar and G. S. Ranganath, Adv. Phys. **35**, 507 (1986).